Chapter 16

Tantalate-based Perovskite for Solar Energy Applications

Yiguo Su, Junyu Lang, Chunfang Du and Xiaojing Wang

Additional information is available at the end of the chapter

http://dx.doi.org/10.5772/61390

Abstract

To realize a sustainable society in the near future, the development of clean, renewable, cheap and sustainable resources and the remediation of environmental pollutions using solar energy as the driving force would be important. During the past few decades, plenty of efforts have been focused on this area to develop solar light active materials to meet the increased energy and environmental crisis. Owning to the unique perovskite-type structure, tantalate-based semiconductors with unable chemical composition show high activities toward the conversion of solar radiation into chemical energy. Moreover, various engineering strategies, including crystal structure engineering, electronic structure engineering, surface/interface engineering, co-catalyst engineering and so on, have been developed in order to modulate the charge separation and transfer efficiency, optical absorption, band gap position and photochemical and photophysical stability, which would open a realm of new possibilities for exploring novel materials for solar energy applications.

Keywords: Tantalate, photocatalysis, solar energy, perovskite

1. Introduction

In view of global energy crisis and environmental pollution, the search for renewable and clean energy resources and the development of eco-friendly systems for environmental remediation have received great attention. Solar energy is the prime renewable source of energy for every life on the earth. The amount of solar energy that strikes the Earth yearly in the form of sunlight is approximately ten thousand times the total energy that is consumed on this planet [1]. However, sunlight is diffuse and intermittent, which impedes its collecting and storage that play critical roles in the full exploitation of its potentials. As one of the most promising solutions for storing and converting solar energy, semiconductor photocatalysis has attracted much

attention, since it provides an environmental benign strategy for splitting water into hydrogen and oxygen, reducing carbon dioxide into useful chemicals and fossil fuels, and completely eliminating all kinds of contaminants under the sunlight illumination under ambient conditions [2–4]. Generally, the fundamental principles of semiconductor photocatalysis have been extensively reported in previous works [5]. A photocatalytic reaction is initiated on the basis of the formation of photogenerated charges (such as electrons and holes) after capture of sunlight by a semiconductor. Consequently, electrons can transit from valence band (VB) to conduction band (CB) leaving behind holes in the VB. If the photogenerated electron–hole pairs' separation is maintained, the photogenerated carriers can move to the semiconductor surfaces to react with the adsorbed small molecules (dioxygen and water), generating the redox foundations of active species which lead to water splitting and/or destruction of organic compounds [6]. It is also noted that the photogenerated electrons in the CB can also recombine with the photogenerated holes in the VB to dissipate the input energy in the form of heat or radiated light (see Figure 1). From the perspective of efficient utilization of solar energy, the recombination between the photogenerated electrons and holes is not desired, which limits the efficiency of a semiconductor photocatalyst. For better photocatalytic performance, the photogenerated electrons and holes must be separated effectively, and charges have to be transferred rapidly at the mean time across the photocatalysis to astrict the recombination.

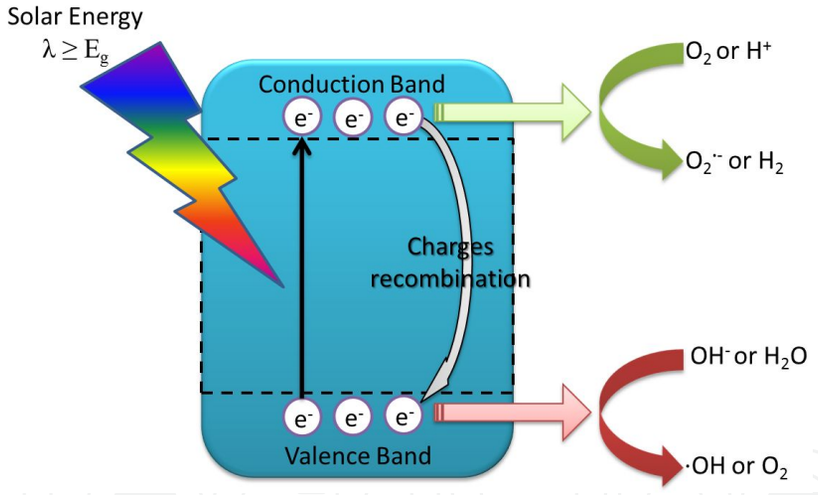

Figure 1. Schematic illustration of the principle of photocatalysis.

To date, several semiconductors, including TiO_2, ZnO, SnO_2, $BiVO_4$ and so forth, have been extensively investigated [7–10]. Among them, tantalate-based semiconductors with perovskite-type structure have certainly verified to be one of the brilliant photocatalysts for producing hydrogen from water and the oxidative disintegration of much organic containment [11]. For instance, $NaTaO_3$ with a perovskite-type structure showed a quantum yield of 56% under ultraviolet light irradiation after lanthanum doping and NiO co-catalyst loading [12]. Nevertheless, because of their broad band gap, most tantalate-based semiconductors can only react under ultraviolet or near-ultraviolet radiation, which reduces the utilization of ~43% of the solar spectrum To efficiently utilize the sunlight in visible region, the design of visible-light

http://dx.doi.org/10.5772/61390

response tantalate-based catalysts is current demanded. Up to now, numerous methodologies have been developed to prepare different visible-light-driven tantalate-based photocatalysts, including doping strategy, heterojunction, facet control and so on [13,14].

This chapter emphasizes certain topical works that concentrate on tantalate-based photocatalysts for solar energy application. The aim is to display that the rational design, fabrication and modifications of tantalate-based semiconductors have tremendous effects onto their final photocatalytic activity, simultaneously, providing some stimulating perspectives on the future applications.

2. Alkali tantalate-based perovskite semiconductors

2.1. Synthetic strategies of alkali tantalates

Alkali tantalate-based perovskite semiconductors (likewise $LiTaO_3$, $NaTaO_3$ and $KTaO_3$) have a general formula of ABO_3 and have drawn a lot of attention due to the peculiar superconductivity, photocatalytic property, electrochemical reduction and electromagnetic features. There are two kinds of totally different cationic sites in a perovskite photocatalysis, in which A-site is coordinated by twelve O^{2-}, and is usually occupied by relative bigger cations (Li, Na and K). The B-site is taken up by smaller cations (Ta) with a coordination of six, as illustrated in Figure 2. The bond angles of Ta–O–Ta are 143° for $LiTaO_3$, 163° for $NaTaO_3$ and 180° for $KTaO_3$, respectively [15]. Wiegel and coworkers have reported the relationship between crystal structures and energy delocalization for alkali tantalates. When the Ta–O–Ta bond angle is close to 180°, the migration of excitation energy can be accelerated and the band gap decreases [16]. Thereby, the delocalization of excited energy of $LiTaO_3$, $NaTaO_3$ and $KTaO_3$ increases in turn. This result suggests that $KTaO_3$ may be predicted to be with the best photocatalytic activity.

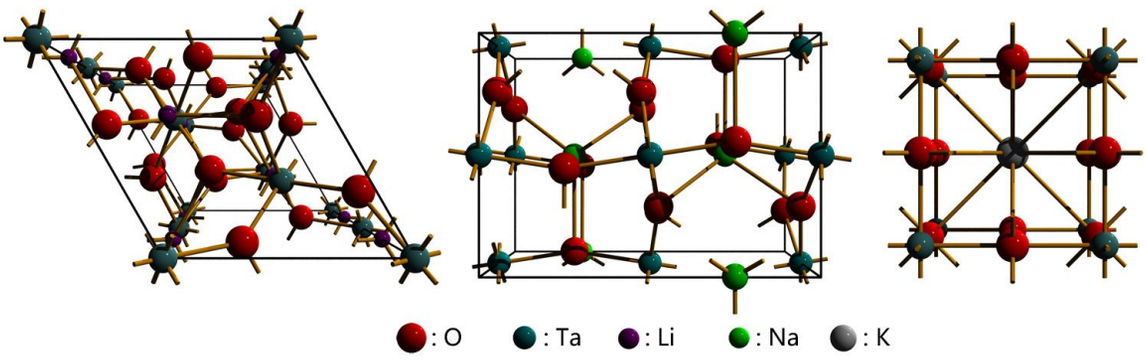

Figure 2. Crystal structure of $LiTaO_3$, $NaTaO_3$ and $KTaO_3$, respectively.

Alkali tantalate with different sizes, morphologies and compositions can be prepared via traditional solid-state method, solvothermal, sol–gel, molten salt and other methods. Basically, the traditional solid-state method is quite often used to prepare alkali tantalates, which

includes the high temperature processing of the combination of alkali salts and tantalum pentaoxide. Kudo and coworkers successfully prepared $ATaO_3$ (A = Li, Na and K) materials with high crystallinity via solid-state method. It is found that all alkali tantalate showed superior photocatalytic activity toward stoichiometric water splitting under ultraviolet condition [17]. The high photocatalytic activity is chiefly depending on the high CB level consisting of Ta 5d orbitals [15]. Among them, $KTaO_3$ is the most photocatalytic active, which may be ascribed to the fact that $KTaO_3$ can absorb the most of photons and possesses the least distorted perovskite structure, being consistent with the above-mentioned discussion. The evolution rate of H_2 and O_2 was determined to be 29 and 13 $\mu molh^{-1}$, respectively. To improve more photocatalytic activity of $ATaO_3$, a modified solid-state method was adopted by adding extra amount of alkali to compensate the loss [18]. When preparing the alkali tantalates with the existence of excess alkali, the photocatalytic activity of $LiTaO_3$, $NaTaO_3$ and $KTaO_3$ materials were improved ten to hundred times. $LiTaO_3$ is the naked alkali tantalate photocatalyst which showed the highest activity. This is because $LiTaO_3$ possesses higher conduction band levels than that of $NaTaO_3$ and $KTaO_3$, which may predict higher transfer rate of excited energy and the subsequent higher phtocatalytic activity. This type of phenomena was likewise observed for $CaTa_2O_6$, $SrTa_2O_6$ and $BaTa_2O_6$ photocatalysts with similar crystal structures [19].

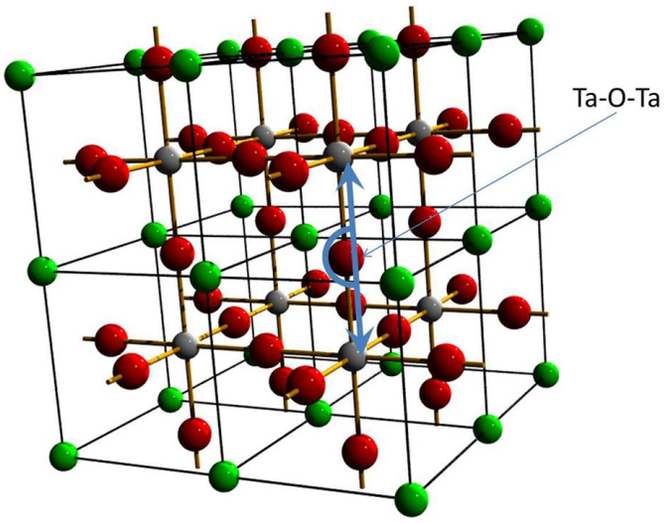

Figure 3. Ta–O–Ta bond angle in a 2 × 2 × 2 supercell of monoclinic phase NaTaO3. Red ball, green ball and grey ball represent O, Na and Ta atoms, respectively.

One should note that the synthetic strategy also has great influence on the structural features as well as photocatalytic activity. For instance, sol–gel method was also used to prepare $NaTaO_3$ nanoparticles. By using $CH_3COONa\ 3H_2O$ and $TaCl_5$ as the raw materials and citric acid as the complexing agent, $NaTaO_3$ nanoparticles with monoclinic phase that shows an indirect band gap, high densities of states near the band edges and a Ta–O–Ta bond angle close to 180° (Figure 3) are obtained. This result is quite different to $NaTaO_3$ that was synthesized via solid-state method, which formed the orthorhombic phase that has a direct band gap and a Ta–O–Ta bond angle of 163°. It is found that monoclinic $NaTaO_3$ has lots of effective states available for the photogenerated charge pairs. Meanwhile, the larger surface area and the

advantageous features in the electronic and crystalline structures for the monoclinic $NaTaO_3$ have resulted in a remarkably higher photocatalytic activity for the sol–gel synthesized $NaTaO_3$ than that for the solid-state derived orthorhombic $NaTaO_3$ [20]. Besides sol–gel method, the molten-salt approach is also adopted to prepare alkali tantalate materials [21,22]. By a convenient molten-salt process, a series of $NaTaO_3$ and $KTaO_3$ efficient photocatalysts is successfully synthesized, which are highly crystallized single crystal nanocubes (about 100 nm large). Doping tetravalent Zr^{4+} and Hf^{4+} in $NaTaO_3$ and $KTaO_3$ efficiently increases the activity and stability of catalyst at the same time, although the energy levels have no change. Moreover, Zr^{4+} and Hf^{4+} doping can also led to particle size reduction and nearly monodispersed feature of $NaTaO_3$ and $KTaO_3$ nanoparticles. In the absence of co-catalyst, the photocatalytic activity can reach 4.65 and 2.31 $mmolh^{-1}$ toward H_2 and O_2 production, respectively [22]. A novel kind of strontium-doped $NaTaO_3$ mesocrystals was also prepared by a common molten-salt way. The obtained three-dimensional architectures showed high crystallinity, preferred orientation growth and high surface area. The ability for hydrogen generation of photocatalyst achieves 27.5 and 4.89 $mmolh^{-1}$ for methanol aqueous solution and pure water splitting under ultra-violet light irradiation [23]. However, either solid-state method or molten-salt approach often leads to ultra-low surface areas of alkali tantalates, which limits the photocatalytic activity. Hydrothermal synthesis is advantageous for regular nucleation of nanocrystals with well-defined particles, morphologies, crystallinity and surface areas [24]. For instance, nano-sized Ta_2O_5 and $NaTaO_3$, $KTaO_3$ and $RbTaO_3$ cubes are prepared by a facile hydrothermal method [25]. It is observed that pH influences much in the process of tantalum compound nanoparticles preparation. The obtained morphologies ranging from agglomerated particles in acidic medium over sticks at neutral pH value to cubes in elementary media can be achieved, which are similar to titanates [26]. A microwave-assisted hydrothermal technique was reported using Ta_2O_5 and NaOH as starting materials under quite mild conditions with short reaction time. The BET surface area of $NaTaO_3$ nanoparticles prepared by microwave-assisted hydrothermal method is about 1.5 times than that prepared by conventional hydrothermal method [27]. After loading NiO as co-catalyst, this photocatalyst showed photocatalytic activity for overall water splitting more than two times greater than those prepared by conventional hydrothermal process [28]. As an outstanding example, $NaTaO_3$ nanoparticles through hydrothermal treatment highly improved the photocatalytic activity by a factor of 8 toward water splitting in comparison with the photocatalysts obtained by traditional solid-state method, which is attributed to their smaller particle size, larger surface area and higher crystallinity [29,30].

2.2. Electronic structure engineering

2.2.1. Doping strategies

Introducing foreign elements, including metal ions or non-metal ions, into semiconductor host matrix is one of the most effective methods to modulate the electronic structure of the host semiconductor and produce enhanced photocatalytic performance. Owing to a big difference in radius of A- and B-site ions in alkali tantalates, the dopants can selectively permeate into the A or B sites, which determine chemical composition, surface features, electronic structure and their photocatalytic properties. To date, studies on the alkali tantalates derived by doping strategy are thoroughly investigated. La-doped $NaTaO_3$ is the most active photocatalyst in

photocatalytically splitting water area [12]. In this case, the catalytic activity of $NaTaO_3$ is extremely modulated by doping with La^{3+}. For example, the crystallinity growths and a surface stair structure with nanometer-scale features are constructed, which improve the separation efficiency of the photogenerated electron–hole pairs and the photocatalytically splitting water activity. The surface step structure is also formed in alkaline earth metal ion doped $NaTaO_3$, which showed improvement of photocatalytic water splitting properties [31]. Bi^{3+} doped $NaTaO_3$ nanoparticles are prepared under different initial stoichiometric ratio by traditional solid-state reaction, which showed visible light absorption and tunable photocatalytic activity. Controlling the original molar ratio of the reactants, the intrusion of bismuth at sodium site and tantalum site in $NaTaO_3$ can be well-modulated and the optimum performance can be easily changed. Occupancy of Bi atom at Na site of $NaTaO_3$ is not contributing to increase visible light absorption while occupancy of Bi at Ta site or at both Na and Ta site induces visible light absorption and the subsequent methyl blue degradation under visible light [32,33]. La, Cr codoping $NaTaO_3$ system is also developed by spray pyrolysis from aqueous and polymeric precursor solution. The hydrogen evolution rate of La, Cr codoped $NaTaO_3$ was enhanced 5.6 times to 1467.5 μmol $g^{-1}h^{-1}$, and the induction period was shortened to 33%, compared to the identical values achieved by the Cr-doped $NaTaO_3$ photocatalyst prepared from aqueous precursor solution [34]. Besides metal ion doping, several non-metal ions are also incorporated into the host matrix of alkali tantalates for improved visible light absorption and photocatalytic performance [35,36]. A plane-wave-based density functional theory calculation is conducted to predict the doping effects on the variations of the band structure of non-metal ions doped $NaTaO_3$. There were studies about nitrogen, sulfur, carbon and phosphorus monodoping and nitrogen–nitrogen, carbon–sulfur, phosphorus–phosphorus and nitrogen–phosphorus codoping. Nitrogen and sulfur monodoping can improve the valence band edge to higher and keep the ability to split water into H_2 and O_2 remain unchanged, as is shown in Figure 4. Double hole-mediated codoping can decrease the band gap dramatically. Nitrogen–nitrogen, carbon–sulfur and nitrogen–phosphorus codoping could narrow band gap to 2.19, 1.70 and 1.34 eV, respectively, which could absorb visible light.

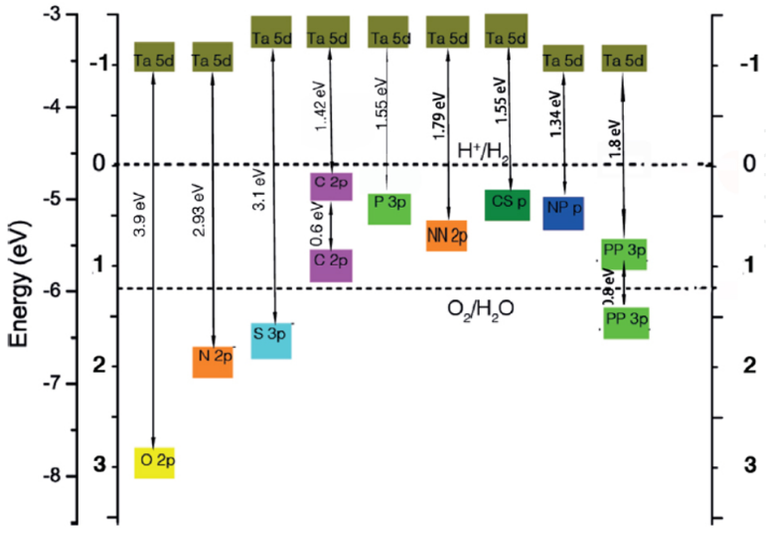

Figure 4. Band alignment of non-metal ions doped $NaTaO_3$. The position of the valence band edge of pure $NaTaO_3$ is adopted from experiment [37].

2.2.2. Defect chemistry engineering

Defect chemistry plays an important role in modulating the electronic structure, charge carrier conductivity and photocatalytic performance [38]. Defect chemistry often shows different impacts on the photocatalytic efficiency for most of the semiconductors. Previous literature on $NaTaO_3$ indicated that the accretion of the extra quantity of Na in the synthesis of $NaTaO_3$ blocked construction of sodium ion defects in $NaTaO_3$ crystals, leading to the extreme enhancement of photocatalytic activity [18]. Basically, the native defects, such as oxygen vacancies and sodium ion defects, are often observed in $NaTaO_3$. Oba and coworkers investigated the formation energies and electronic structure of lattice vacancies, antisite defects and lanthanum impurities in $NaTaO_3$ using first-principles calculations based on density-functional theory [39]. Under oxygen-poor environments, oxygen vacancy as a double donor is a main defect. In La-$NaTaO_3$, the replacement of La at Ta site is similar to make up as a shallow acceptor under oxygen-rich environments whereas the replacement of La at Na site forms as a double donor under oxygen-poor environments. The location predilection of lanthanum leads to self-compensation in heavily doped cases, which have great impact on the change in carrier concentration and photocatalytic activity [12]. Defective center not only alters the carrier concentration but also induces visible light absorption. In Eu^{3+} doped $NaTaO_3$, a nonstoichiometric Na/Ta molar ratio led to site-selective occupation of Eu^{3+} dopant ions, which resulted in a monotonous lattice expansion and local symmetry distortion [11]. The site-selective occupation of Eu^{3+} gave rise to certain types of defective centers due to the charge difference between Eu^{3+} ions and Na^{+} and/or Ta^{5+} ions, which is crucial to the modification of absorption in visible region and photocatalytic activity.

2.3. Surface/interface engineering

2.3.1. Heterojunction of nano-/microarchitectures

The constructions of heterojunction by combining a semiconductor with other semiconductors have attracted much research attention because of their perfect effectiveness in the separation of the photogenerated charge carriers and boosting the photocatalytic activity. In the past few years, a lot of significant findings have been described on the heterojunction of nano-/microarchitectures. Nano-Cu_2O/$NaTaO_3$ composite for the degradation of organic pollutants have also been successfully developed [13]. Nano-Cu_2O/$NaTaO_3$ composite exhibits highly enhanced photocatalytic activity in comparison to their individual counterpart. Furthermore, C_3N_4/$NaTaO_3$ and C_3N_4/$KTaO_3$ composite photocatalysts were also developed [40,41]. Loading of C_3N_4 is a good strategy to achieve the visible light photocatalytic activity (Figure 5). Photogenerated electron jumped from the VB to CB of C_3N_4 could unswervingly insert into the conduction band of $NaTaO_3$ or $KTaO_3$, making C_3N_4/$NaTaO_3$ and C_3N_4/$KTaO_3$ as visible light-driven photocatalyst. Both of the composites showed superior photocatalytic activity toward Rhodamine B degradation under visible light irradiation, being close to commercial P25. Yin and coworkers reported the preparation of novel C–$NaTaO_3$–Cl–TiO_2 composites via a facile solvothermal method. When C–$NaTaO_3$ is joined with Cl–TiO_2 to construct a core shell configuration, the visible light-induced degradation activity toward NO_x of the catalysts under

visible light irradiation could be highly improved because of the suppression of the recombination of photogenerated charge carriers [42]. Zaleska et al. prepared a series of novel binary and ternary composite photocatalysts based on the combination of $KTaO_3$, CdS and MoS_2 semiconductors via hydro/solvothermal precursor route. They found that the highest photocatalytic activity toward phenol degradation under both UV-Vis and visible light irradiation and superior stability in toluene removal was observed for ternary hybrid obtained by calcination of $KTaO_3$, CdS and MoS_2 powders at the 10: 5: 1 molar ratio [43].

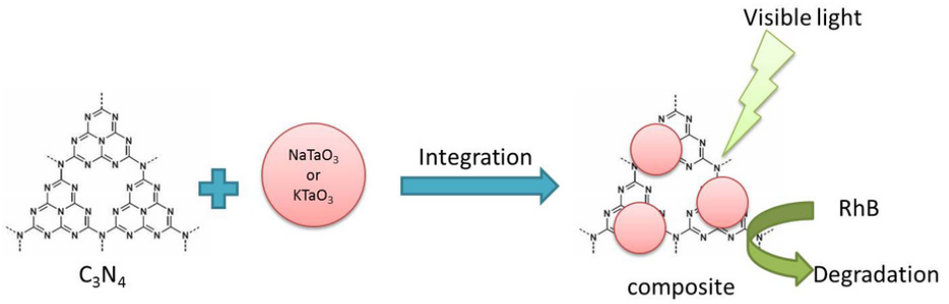

Figure 5. Schematic illustration of the photocatalytic degradation process of RhB by visible light-irradiated C_3N_4/$NaTaO_3$ or C_3N_4/$KTaO_3$.

2.3.2. Mesoporous structures construction

As one of the most important factors, surface area also imposes a big effect on the photocatalytic activity of the semiconductors. The majority of photocatalytic reactions occur at semiconductor surfaces, and therefore the photocatalytic activities of semiconductor oxides are usually greatly improved by the increase in surface area [44]. To further improve the surface area, nanocrystalline $NaTaO_3$ thin films with ordered three-dimensional mesoporous and nanostick-like constructions were successfully produced by PIB-*b*-PEO polymer-based sol–gel method. $NaTaO_3$ prepared at 650°C exhibits a BET surface area of about 270 m^2cm^{-3}, which is much larger than the ever reported values [45]. These nanocrsytalline mesoporous $NaTaO_3$ samples show both enhanced ultraviolet light photocatalytic activity and can keep steady performance. A confined space synthesis process was also used for preparing colloidal array of $NaTaO_3$ by using three-dimensional mesoporous carbon as the hard template. This method brings about the creation of a colloidal collection of mesoporous $NaTaO_3$ particles (20 nm). After NiO loading, the mesoporous $NaTaO_3$ nanoparticles showed photocatalytic activity for overall water splitting more than three times as high as non-structured bulk $NaTaO_3$ particles [46]. A carbon modified $NaTaO_3$ mesocrystal nanoparticle was also successfully synthesized by a one-pot solvothermal method by employing $TaCl_5$, NaOH and glucose as the starting materials and distilled H_2O/ethylene glycol mixed solution as a reaction solvent. The as-synthesized mesocrystal nanoparticles exhibited a high specific surface area of 90.8 m^2g^{-1} with large amounts of well-dispersed mesopores in the particles. The carbon-modified $NaTaO_3$ mesocrystal demonstrated excellent efficiency for continuous NO gas destruction under visible light irradiation, which is considerably superior to those of the unmodified $NaTaO_3$ specimen and

commercial Degussa P25, owning to large specific surface area, high crystallinity and visible light absorption [47].

2.4. Co-catalyst engineering

2.4.1. Noble metal co-catalyst engineering

As well documented in previous literatures, co-catalyst introduces two positive factors into the photocatalyst, including promotion on the separation of photogenerated charge carriers and construction of active sites for reduction and/or oxidation reaction. Several noble metals have been commonly used as co-catalysts for photocatalytic applications. For example, water splitting activity of $NaTaO_3$:La was improved when Au was loaded either by photodeposition method or by impregnation method. Moreover, Au/$NaTaO_3$:La prepared by impregnation method exhibits much higher and more stable photocatalytic activity toward water splitting due to the fact that O_2 reduction on photodeposited Au co-catalyst was more efficient than that of impregnated Au co-catalyst [48]. Besides Au nanoparticles, Pt is also frequently used as co-catalyst for increasing the photocatalytic activity of alkali tantalates. With the deposition of Pt nanoparticles as co-catalyst, rare earth (including Y, La, Ce and Yb) doped $NaTaO_3$ exhibits a clear improvement of the hydrogen evolution, which is due to the fact that Pt nanoparticles act as electron scavengers reducing the photogenerated charge carrier recombination rate and facilitating the electron move to metal sites from the CB of $NaTaO_3$, being as the catalytic center for hydrogen generation [49]. Moreover, Pd nanoparticles are also used as a co-catalyst for H_2 production from water containing electron donor species. Su et al. prepared novel Pd/NiO core/shell nanoparticles as co-catalyst, which are placed on the surface of La doped $NaTaO_3$ photocatalyst. It is noted that Pd nanoparticles are more effective for H_2 generation from water containing methanol, while Pd/NiO core/shell nanoparticles exhibit a higher H_2 generation by splitting pure water. The presence of NiO not only provides hydrogen evolution sites and suppresses the reverse reactions on Pd-based catalysts but also improves the stability of the Pd nanoparticles on the La doped $NaTaO_3$ surfaces [50]. In another case, when RuO_2 (1 wt.%) was introduced as co-catalyst, the ability for H_2 generation of $NaTaO_3$ prepared by an innovative solvo-combustion reaction was improved significantly, reaching around 50 mmol of H_2 after 5 h, which is the best of other reports in literature [51].

2.4.2. Earth abundant elements co-catalyst engineering

Due to too much scarcity and expense of noble metal co-catalyst to apply for wider scope solar energy applications, the development of high-efficiency and low-cost noble-metal-free co-catalysts is acutely necessary. Lately, co-catalysts composed of earth abundant elements have been explored extensively to replace noble metal co-catalysts for solar energy applications [52]. NiO is a p-type semiconductor with a band gap energy ranging within 3.5–4.0 eV, which is widely used as the co-catalyst of tantalates-based semiconductors for enhancing photocatalytic activity [53]. In the case of NiO/$NaTaO_3$:La photocatalyst with high photocatalytic reactivity, NiO acts as co-catalyst loading as ultrafine NiO particles, which possesses characteristic absorption bands at 580 and 690 nm, The ultrafine NiO particles were highly active for

hydrogen evolution as well as Pt of an excellent co-catalyst [12]. A detailed study on the structural features of NiO nanoparticles indicated that the interdiffusion of Na^+ and Ni^{2+} cations created a solid–solution transition zone on the outer sphere of $NaTaO_3$. The high photocatalytic activity resulting from a low NiO loading suggests that the interdiffusion of cations heavily doped the p-type NiO and n-type $NaTaO_3$, reducing the depletion widths and facilitating charge transfers through the interface barrier [54]. Besides NiO, Ni metallic nanoclusters were also used as co-catalyst. For instance, a series of nickel-loaded $La_xNa_{1-x}TaO_3$ photocatalysts was synthesized by a hydrogen peroxide-water based solvent method. Systematical investigation indicated that the activity of hydrogen generation from pure water is in sequence: Ni/NiO > NiO > Ni, whereas the activity sequence with respect to aqueous methanol is: Ni > Ni/NiO > NiO. Ni metallic nanoclusters exhibit the most active sites and facilitate the formation of hydrogen from aqueous methanol. In the case of Ni/NiO core/shell structure, Ni metallic nanoclusters induce the migration of photogenerated electrons from the bulk to catalyst surface, while NiO acts as H_2 evolution site and prevents water formation from H_2 and O_2 [55].

2.4.3. Molecular co-catalyst engineering

Molecular co-catalyst engineering have received much research attention in recent years. In a molecular/semiconductor hybrid system, the noble-metal-free molecular complex as co-catalyst can not only facilitate the charge separation but also help us to understand the mechanisms of hydrogen evolution and carbon dioxide reduction at molecular level [56]. Although the study on molecular sensitized alkali tantalates is limited, an excellent research has been done by Hong and coworkers. In this case, by using a molecular co-catalyst $[Mo_3S_4]^{4+}$, the photocatalytic activity of $NaTaO_3$ was significantly improved. The hydrogen production rate is about 28 times higher than pure $NaTaO_3$ because $[Mo_3S_4]^{4+}$ clusters can provide a large number of effective active sites for hydrogen evolution and the matching of the conduction band of $NaTaO_3$ and the reduction potential of $[Mo_3S_4]^{4+}$ also acts as one of the major determinants for the enhancement of the photocatalytic activity [57].

3. Alkaline earth and transition metal tantalate-based perovskite semiconductors

3.1. Synthetic methodologies of alkaline earth and transition metal tantalates

Solid-state reaction method and hydrothermal method are used routinely to synthesize alkaline earth and transition metal tantalates. Almost all the alkaline earth and transition metal tantalates can be obtained by high-temperature solid-state method using Ta_2O_5 and other salts as starting materials. For instance, $Sr_2Ta_2O_7$ [58], $Sr_{0.8}Bi_{2.2}Ta_2O_9$ [59], $Bi_2SrTa_2O_9$ [60] $H_{1.81}Sr_{0.81}Bi_{0.19}Ta_2O_7$ [61], $Ba(Zn_{1/3}Ta_{2/3})O_3$ [62], $Ba(Mg_{1/3}Ta_{2/3})O_3$ [63], $Ba_4Ta_2O_9$ [64] and $Ba_5Ta_4O_{15}$ [65] have been synthesized successfully by this method, which show prospects in many application including photocatalytic semiconductor, solar cells and electronic device. The high-temperature treatment of traditional solid-state reaction will increase the size of particles and thus decrease the surface area. $Sr_2Ta_2O_7$ photocatalysts of layered perovskite

structures gotten from the solid state reaction had better activity which is mainly because of their more negative conduction band. $H_2ATa_2O_7$ (A = Sr or $La_{2/3}$) [66] and $LiCa_2Ta_3O_{10}$ [67] were reported to be obtained by similar way with extra alkali, which can supply the loss at high temperature to suppress defects formation. This makes the crystal structure grow well and has better catalytic efficiency than others synthesized with a theoretical ratio in most cases. This improved solid-state reaction method would efficiently inhibit the recombination of photocarrier to enhance the photocatalytic activity. A new polymerizable complex technique is one of the preparation methods of alkaline earth tantalates, which has a relative moderate condition. This method includes the provision of Ta-base compound and then come into being the sticky sol–gel, after the treatment at 600–700 °C. Comparing with solid-state method, the tantalate-based photocatalysts synthesized by a polymerizable complex way often have greater crystallinity and better crystal size, which will lead to remarkably increase the photocatalytic efficiency [68]. Comparing with solid-state method, hydrothermal method has been widely used in synthesizing perovskite tantalates with very lower reaction temperature. Lots of alkaline earth tantalate could be prepared by the hydrothermal method exhibiting higher activity. In 2006, Zhu and coworkers synthesize monomolecular-layer $Ba_5Ta_4O_{15}$ nanosheets by hydrothermal method [65], which show enhanced activity ten times better than that of solid-state method-derived $Ba_5Ta_4O_{15}$ particles in photodegradation reactions of Rhodamine B solution. Perovskite $Ca_2Ta_2O_7$ has also been synthesized by hydrothermal process in aqueous KOH solution at 373 K for 120 h, which shows photocatalytic water splitting activity under UV-light irradiation [69]. Moreover, sol–gel route, as a common way to prepare the nanomaterials, also can be used for preparation of some perovskite tantalates. One typical case is that the ferroelectric $SrBi_2Ta_2O_9$ [70] and $SrBi_2Ta_2O_9$ nanowires [71] were synthesized using ethylene glycol as solvent, which showed greater dielectric and ferroelectric properties than the ceramics prepared by the solid-state reactions owning to a denser and more homogeneous microstructure with a better distribution of grain orientations. Sol–gel method is also used to prepare metastable phase like $Sr_{0.5}TaO_3$ nanosheets [72] with photocatalytic activities of water splitting under ultraviolet light irradiation. Several transition metal tantalates with perovskite structure can also be synthesized by these methods, including $AgTaO_3$ [73], $LaTaO_4$ [74], $H_2La_{2/3}Ta_2O_7$ [75] and so forth.

3.2. Crystal structure engineering

For ideal perovskite alkaline earth and transition metal tantalates, the cubic-symmetry structure has the Ta atom in 6-fold coordination, surrounded by an octahedron of oxygen atoms, and the alkaline earth or transition metal cation in 12-fold cuboctahedral coordination (Figure 6). The relative ion size requirements for stability of the cubic structure are quite stringent, so slight buckling and distortion can produce several lower-symmetry distorted versions, in which the coordination numbers of cations are reduced. [77] But in fact, almost all perovskite alkaline earth and transition metal tantalates have compound perovskite structures covering two different cations at Ta site in TaO_6 octahedra or at cation site in 12-fold cuboctahedral coordination. This led to the chance of alternatives between ordered and disordered. Crystal structure is a very important factor manipulating the band gaps of perovskite tantalates containing the following aspects: (1) the bond angle of tantalum and oxygen ions of octahedra

units; (2) the interlayer spacing of the perovskite; (3) the interaction between perovskite layers; (4) the polarization ability of cations at the interlayer toward the oxygen ions of octahedra facing the interlayer. Some of alkaline earth and transition metal tantalates with layered perovskite exhibited outstanding photo catalytic activity, including $Ba_5Ta_4O_{15}$, $H_{1.81}Sr_{0.81}Bi_{0.19}Ta_2O_7$, $SrBi_2Ta_2O_9$, $LaTaO_4$, $H_2La_{2/3}Ta_2O_7$ and $Sr_{0.5}TaO_3$ reported by many groups [61,65,70,72,74,75]. This kind of perovskite composites are promising materials with multiple elements, perovskite framework and layer-like structures, which can be classified into three category structures by the different interlayer structure. On the other hand, it has been reported that some perovskite alkaline earth tantalates with double-perovskite structure also show photocatalytic activity under ultraviolet light irradiation [79]. And some transition metal tantalates have simple cubic perovskite-type structure like $AgTaO_3$, $Ba_3ZnTa_2O_9$, Sr_2GaTaO_6 [80] and $NaCaTiTaO_6$, $NaCaTiNbO_6$, $NaSrTiTaO_6$ and $NaSrTiNbO_6$ [81].

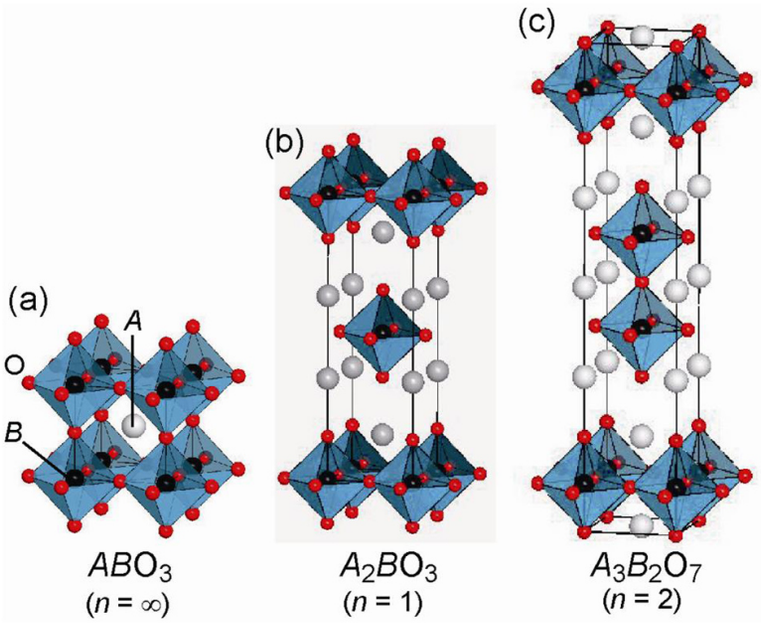

Figure 6. General structure of perovskite and layered perovskite [76].

3.3. Metal/non-metal doping strategies for band gap engineering

Introducing external ions into crystal structure has been generally approved as a positive way to improve the visible-light photocatalytic activity of semiconductors with larger band gaps. For nitrogen-doped layered oxide $Sr_5Ta_4O_{15-x}N_x$, the extension of the visible light absorption has been ascribed to the substitution of nitrogen for oxygen atoms as well as the formation of Ta–N bonds. The N 2p states mixed with pre-existing O 2p states shift the valence band maximum upward and result in wide visible light absorption [82]. A slight N dopant led to hinder the recombination of photo-generated charge pairs. N-doped $Ba_5Ta_4O_{15}$ also displays a brilliant photocatalytic activity under solar condition. The doping resulted in a significant narrowing of the band gap from 4.06 eV to ca. 1.76 eV, indicating that it can use more visible

http://dx.doi.org/10.5772/61390

light [83]. Furthermore, Sun et al. investigated affection of band gap doping with several metal and non-metal by DFT calculation [84]. It is found that, in most perovskite cases, the valence band levels were shifted upwards, in which the maximum contribution to valence band maximum comes from the p orbitals of the dopant anions, which shift. On the other hand, the dopant cations shift the CB level downwards because the CBM is chiefly governed by the d orbitals of foreign cations. This conclusion was applicable to perovskite structure tantalates system (Figure 7) directly by Liu and coworkers [85].

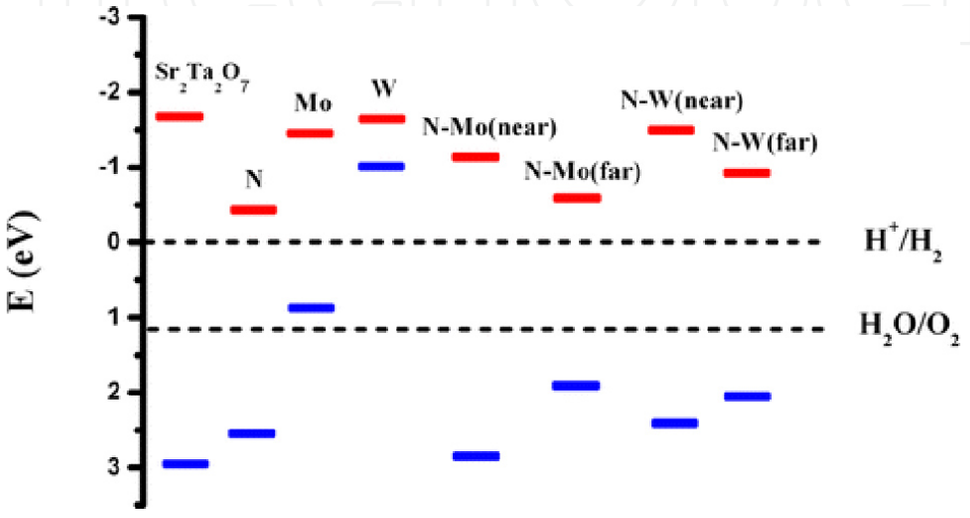

Figure 7. The electronic band edge positions with respect to the water reduction and oxidation potential levels for the pure and doped $Sr_2Ta_2O_7$ systems [85].

3.4. Multi-component heterojunction

Multi-component semiconductor combination tactic shows effectivity to improve photocatalytic activity by separation of the photo-generated charge carriers with a formation of a heterojunction structure. Heterojunction structure is the interface that is located at two areas of different crystalline semiconductors. This kind of material has to consider the following points, including near crystal structure, similar interatomic spacing and close coefficient of thermal expansion. Otherwise, they should have discrepant band gap values, which is exact contrary to a homojunction. It is benefited to regulate the electronic energy bands. To promote the redox ability and photocatalytic activity, composite photocatalysts involving two or more components were extensively studied. One type of such composites is usually constructed by coupling semiconductors with larger band gap for the purpose of the higher redox ability. A charming work is the $Ba_5Ta_4O_{15}/Ba_3Ta_5O_{15}$ composite reported by Roland Marschall et al., which synthesized through the sol–gel method showed brilliant activities in OH radical generation and photocatalytic hydrogen production [86]. The outstanding activity is expected to come from enhanced charge carrier separation. In 2011, Wang and coworkers present Pt-loaded graphene-$Sr_2Ta_2O_{7-x}N_x$ (Figure 8) with enlarged visible light absorption region and enhanced photocatalytic hydrogen generation [87].

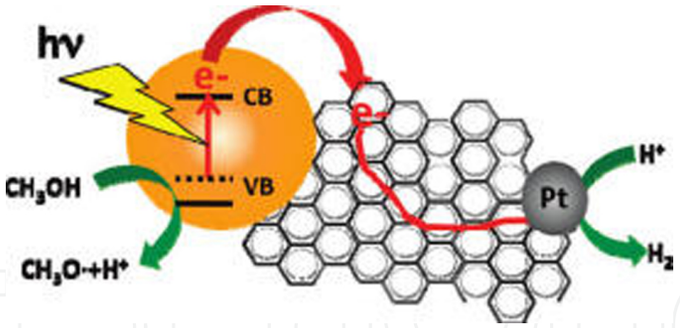

Figure 8. Schematic diagram for Pt-loaded graphene-$Sr_2Ta_2O_{7-x}N_x$ photocatalyst under simulated solar light irradiation [87].

3.5. Co-catalyst surface modification

Transition metals and their oxides are usually used as practical co-catalysts for photocatalysis. The role of the co-catalysts attached on the surface of the semiconductor material is particularly significant. It increases the overall photocatalytic activity by helping to separate charge pairs, which can work for both bulk and surface electron/hole pathway. The chemical reaction that took place at surface is promoted by the co-catalysts. Various metals and oxides loaded on the surface of semiconductor show different effects. In most photocatalytic water splitting systems, several metals like Au and Pt can accelerate the rate of reduction of hydrogen observably [88, 89]. On the other hand, some oxides like NiO, NiO_x and RuO_2 can promote the rates of both hydrogen and oxygen production [90–92]. Among them, NiO_x exhibited highest activity in photocatalytic process [78]. As a hydrogen evolution site, the co-catalyst has to extract the photogenerated electrons from the CB of host materials. Thus, the conduction band level of co-catalyst should be below that of photocatalyst. In addition, photocatalytic water splitting is sensitive to the deposition methods of co-catalysts. Kudo et al. reported that photocatalysts show diversity in photocatalytic water splitting with different deposition methods [59]. Moreover, transition-metal sulfides like MS (M = Ni, Co, Cu) have also been developed as co-catalysts to improve the photocatalytic activity. These sulfides have the same effects with other co-catalysts in reaction process [93].

4. Summary and outlook

Tantalate-based perovskite semiconductors are well known for their wide spread applications in photocatalysis, ionic conductors, luminescence host materials and ferroelectric ceramics. Drawbacks of wide band gap and low charge separation efficiency inhibit the further development of tantalate-based perovskite semiconductors as superior photocatalysts. The combination of various strategies, such as doping, heterojunction and co-catalyst engineering, induces a thrilling beginning for exploring visible light active and highly efficient photocatalysts for solar energy applications. However, the studies on tantalate-based perovskite semiconductors are currently unsystematic. Meanwhile, the as-mentioned strategies and the derived photocatalytic systems with high efficiency and stability still need to be further developed.

Acknowledgements

This work is financially supported by the National Natural Science Foundation of China (Grants 21267014, 21367018, 21563021), the Project of Scientific and Technological Innovation Team of Inner Mongolia University (12110614), Fund of Key Laboratory of Optoelectronic Materials Chemistry and Physics, Chinese Academy of Sciences (2008DP173016-1410).

Author details

Yiguo Su, Junyu Lang, Chunfang Du and Xiaojing Wang*

*Address all correspondence to: wang_xiao_jing@hotmail.com

College of Chemistry and Chemical Engineering, Inner Mongolia University, Hohhot, Inner Mongolia, P. R. China

References

[1] Chen HM, Chen CK, Liu RS, Zhang L, Zhang J, Wilkinson DP. Nano-architecture and material designs for water splitting photoelectrodes. Chem Soc Rev 2012;41:5654–71. DOI: 10.1039/C2CS35019J

[2] Martindale BCM, Hutton GAM, Caputo CA, Reisner E. Solar hydrogen production using carbon quantum dots and a molecular nickel catalyst. J Am Chem Soc 2015;137:6018–25. DOI: 10.1021/jacs.5b01650

[3] Tu W, Zhou Y, Zou Z. Photocatalytic conversion of CO_2 into renewable hydrocarbon fuels: state-of-art accomplishment, challenges, and prospects. Adv Mater 2014;26:4607–26. DOI: 10.1002/adma.201400087

[4] Lin Y, Li D, Hu J, Xiao G, Wang J, Li W, Fu X. Highly efficient photocatalytic degradation of organic pollutants by PANI-modified TiO_2 composite. J Phys Chem C 2012;116:5764–72. DOI: 10.1021/jp211222w

[5] Cargnello M, Diroll BT. Tailoring photocatalytic nanostructures for sustainable hydrogen production. Nanoscale 2014;6:97–105. DOI: 10.1039/C3NR05383K

[6] Li L, Liu J, Su Y, Li G, Chen X, Qiu X, Yan T. Surface doping for photocatalytic purposes: relations between particle size, surface modifications, and photoactivity of SnO_2:Zn^{2+} nanocrystals. Nanotechnology 2009;20:155706–9. DOI: http://dx.doi.org/10.1088/0957-4484/20/15/155706

[7] Lin H, Li L, Zhao M, Huang X, Chen X, Li G, Yu R. Synthesis of high-quality brookite TiO_2 single-crystalline nanosheets with specific facets exposed: tuning catalysts from inert to highly reactive. J Am Chem Soc 2012;134:8328–31. DOI: 10.1021/ja3014049

[8] Schumann J, Eichelbaum M, Lunkenbein T, Thomas N, Galván MCÁ, Schlögl R, Behrens M. Promoting strong metal support interaction: doping ZnO for enhanced activity of Cu/ZnO:M (M = Al, Ga, Mg) catalysts. ACS catalysis. 2015;5:3260–70. DOI: 10.1021/acscatal.5b00188

[9] Long J, Xue W, Xie X, Gu Q, Zhou Y, Chi Y, Chen W, Ding Z, Wang X. Sn^{2+} dopant induced visible-light activity of SnO_2 nanoparticles for H_2 production. Catal Commun 2011;16:215–9. DOI: 10.1016/j.catcom.2011.10.002

[10] Thalluri SM, Hussain M, Saracco G, Barber J, Russo N. Green-synthesized $BiVO_4$ oriented along {040} facets for visible-light-driven ethylene degradation. Indust Eng Chem Res 2014;53:2640–6. DOI: 10.1021/ie403999g

[11] Su Y, Peng L, Guo J, Huang S, Lv L, Wang X. Tunable optical and photocatalytic performance promoted by nonstoichiometric control and site-selective codoping of trivalent ions in $NaTaO_3$. J Phys Chem C 2014;118:10728–39. DOI: 10.1021/jp412236u

[12] Kato H, Asakura K, Kudo A. Highly efficient water splitting into H_2 and O_2 over lanthanum-doped $NaTaO_3$ photocatalysts with high crystallinity and surface nanostructure. J Am Chem Soc 2003;125:3082–9. DOI: 10.1021/ja027751g

[13] Su Y, Lang J, Cao N, Wang T, Zhu B, Wang X. Morphological reconstruction and photocatalytic enhancement of $NaTaO_3$ nanocrystals via Cu_2O loading. J Nanoparticle Res 2015;17:63–9. DOI: 10.1007/s11051-015-2877-9

[14] Wang B, Kanhere PD, Chen Z, Nisar J, Pathak B, Ahuja R. Anion-doped $NaTaO_3$ for visible light photocatalysis. J Phys Chem C 2013;117:22518–24. DOI: 10.1021/jp407025r

[15] Kato H, Kudo A. Photocatalytic water splitting into H_2 and O_2 over various tantalate photocatalysts. Catal Today 2003;78:561–9. DOI: 10.1016/S0920-5861(02)00355-3

[16] Wiegel M, Emond MHJ, Stobbe ER, Blasse G. Luminescent of alkali tantalates and niobates. J Phys Chem Solid 1994;55:773–8. DOI: 10.1016/0022-3697(94)90030-2

[17] Kato H, Kudo A. New tantalate photocatalysts for water decomposition into H_2 and O_2. Chem Phys Lett 1998;295:487–92. DOI: 10.1016/S0009-2614(98)01001-X

[18] Kato H, Kudo A. Water splitting into H_2 and O_2 on alkali tantalate photocatalysts $ATaO_3$ (A = Li, Na, and K). J Phys Chem B 2001;105:4285–92. DOI: 10.1021/jp004386b

[19] Kato H, Kudo A. Photocatalytic decomposition of pure water into H_2 and O_2 over $SrTa_2O_6$ prepared by a flux method. Chem Lett 1999;28:1207–8. DOI: 10.1246/cl.1999.1207

[20] Hu CC, Teng H. Influence of structural features on the photocatalytic activity of $NaTaO_3$ powders from different synthesis methods. Appl Catal A: Gen 2007;331:44–50. DOI: 10.1016/j.apcata.2007.07.024

[21] Lee S, Teshima K, Mizuno Y, Yubuta K, Shishido T, Endo M, Oishi S. Growth of well-developed sodium tantalate crystals from a sodium chloride flux. Cryst Eng Comm 2010;12:2871–7. DOI: 10.1039/b921092j

[22] Sun J, Chen G, Li Y, Jin R, Wang Q, Pei J. Novel (Na, K)TaO_3 single crystal nanocubes: Molten salt synthesis, invariable energy level doping and excellent photocatalytic performance. Energy Environ Sci 2011;4:4052–60. DOI: 10.1039/c1ee01259b

[23] Sun J, Chen G, Pei J, Jin R, Wang Q, Guang X. A simple approach to strontium sodium tantalite mesocrystals with ultra-high photocatalytic properties for water splitting. J Mater Chem 2012;22:5609–14. DOI: 10.1039/c2jm16387j

[24] Su Y, Li L, Li G. Synthesis and optimum luminescence of $CaWO_4$-based red phosphors with codoping of Eu^{3+} and Na^{+}. Chem Mater 2008;20:6060–7. DOI: 10.1021/cm8014435

[25] Gömpel D, Tahir MN, Panthöfer M, Mugnaioli E, Brandscheid R, Kolb U, Tremel W. Facile hydrothermal synthesis of crystalline Ta_2O_5 nanorods, $MTaO_3$ (M = H, Na, K, Rb) nanoparticles and their photocatalytic behaviour. J Mater Chem A 2014;2:8033–40. DOI: 10.1039/c4ta00183d

[26] Koll D, Andrusenko I, Mugnaioli E, Birkel A, Panthöfer M, Kolb U, Tremel W. Snapshots of the formation of $NaTi_3O_6(OH)$ $2H_2O$ nanowires: a time-resolved XRD/HRTEM study. Zeitschrift für anorganische und allgemeine Chemie. 2013;639:2521–6. DOI: 10.1002/zaac.201300411

[27] Yin S. Microwave-assisted hydrothermal synthesis of nitrogen doped titania nanoparticles. Funct Mater Lett 2008;01:173 DOI: 10.1142/S1793604708000319

[28] Shi J, Liu G, Wang N, Li C. Microwave-assisted hydrothermal synthesis of perovskite $NaTaO_3$ nanocrystals and their photocatalytic properties. J Mater Chem 2012;22:18808–13. DOI: 10.1039/c2jm33470d

[29] Lee Y, Watanabe T, Takata T, Hara M, Yoshimura M, Domen K. Hydrothermal synthesis of fine $NaTaO_3$ powder as a highly efficient photocatalyst for overall water splitting. Bull Chem Soc Jpn 2007;80:423–8. DOI: 10.1246/bcsj.80.423

[30] Liu JW, Chen G, Li ZH, Zhang ZG. Hydrothermal synthesis and photocatalytic properties of $ATaO_3$ and $ANbO_3$ (A = Na and K). Int J Hydrogen Energy 2007;32:2269–72. DOI: 10.1016/j.ijhydene.2006.10.005

[31] Iwase A, Kato H, Kudo A. The effect of alkaline earth metal ion dopants on photocatalytic water splitting by $NaTaO_3$ powder. Chem Sus Chem 2009;2:873–7. DOI: 10.1002/cssc.200900160

[32] Kanhere PD, Zheng J, Chen Z. Site specific optical and photocatalytic properties of bi-doped $NaTaO_3$. J Phys Chem C 2011;115:11846–53. DOI: 10.1021/jp2003936

[33] Kanhere P, Tang Y, Zheng J, Chen Z. Synthesis, photophysical properties, and photocatalytic applications of Bi doped $NaTaO_3$ and Bi doped $Na_2Ta_2O_6$ nanoparticles. J Phys Chem Solid 2013;74:1708–13. DOI: 10.1016/j.jpcs.2013.06.013

[34] Kang HW, Lim SN, Park SB, Park AA. H_2 evolution under visible light irradiation on La and Cr co-doped $NaTaO_3$ prepared by spray pyrolysis from polymeric precursor. Int J Hydrogen Energy 2013;38:6323-6334. DOI: http://dx.doi.org/10.1016/j.ijhydene.2013.03.048

[35] Li FF, Liu DR, Gao GM, Xue B, Jiang YS. Improved visible-light photocatalytic activity of $NaTaO_3$ with perovskite-like structure via sulfur anion doping. Appl Catal B Environ 2015;166–167:104–11. DOI: 10.1016/j.apcatb.2014.10.049

[36] Liu DR, Jiang YS, Gao GM. Photocatalytic degradation of an azo dye using N-doped $NaTaO_3$ synthesized by one-step hydrothermal process. Chemosphere. 2011;83:1546–52. DOI: 10.1016/j.chemosphere.2011.01.033

[37] Wang B, Kanhere PD, Chen Z, Nisar J, Pathak B. Anion-doped $NaTaO_3$ for visible light photocatalysis. J Phys Chem C 2013;117:22518–24. DOI: 10.1021/jp407025

[38] Chen S, Wang LW. Intrinsic defects and electronic conductivity of TaON: First-principles insights. Appl Phys Lett 2011;99:222103–3. DOI: 10.1063/1.3664346

[39] Choi M, Oba F, Tanaka I. First-principles study of native defects and lanthanum impurities in $NaTaO_3$. Phys Rev B 2008;78:014115–8. DOI: 10.1103/PhysRevB.78.014115

[40] Yong Z, Ren J, Hu H, Li P, Ouyang S, Xu H, Wang D. Synthesis, characterization, and photocatalytic of g-C_3N_4/$KTaO_3$ composites under visible light irradiation. J Nanomater 2015;2015:821986–7. DOI: 10.1155/2015/821986

[41] Kumar S, Kumar B, Surendar T, Shanker V. g-C_3N_4/$NaTaO_3$ organic-inorganic hybrid nanocomposite: high-performance and recyclable visible light driven photocatalyst. Mater Res Bull 2014;49:310–8. DOI: 10.1016/j.materresbull.2013.09.013

[42] Wu X, Yin S, Dong Q, Sato T. Preparation and visible light induced photocatalytic activity of C-$NaTaO_3$ and C-$NaTaO_3$-Cl-TiO_2 composite. Phys Chem Chem Phys 2013;15:20633–40. DOI: 10.1039/c3cp53437e

[43] Bajorowicz B, Cybula A, Winiarski MJ, Klimczuk T, Zaleska A. Surface properties and photocatalytic activity of $KTaO_3$, CdS, MoS_2 semiconductors and their binary and ternary semiconductor composites. Molecules 2014;19:15339–60. DOI: 10.3390/molecules190915339

[44] Su Y, Hou L, Du C, Peng L, Guan K, Wang X. Rapid synthesis of Zn^{2+} doped $SnWO_4$ nanowires with the aim of exploring doping effects on highly enhanced visible photocatalytic activities. RSC Adv 2012;2:6266–73. DOI: 10.1039/c2ra20401k

[45] Reitz C, Brezesinski K, Haetge J, Perlinch J, Brezesinski T. Nanocrystalline $NaTaO_3$ thin film materials with ordered 3D mesoporous and nanopillar-like structures through PIB-*b*-PEO polymer templating: towards high-performance UV-light photocatalysts. RSC Adv 2012;2:5130–3. DOI: 10.1039/c2ra20203d

[46] Yokoi T, Sakuma J, Maeda K, Domen K, Tatsumi T, Kondo JN. Preparation of a colloidal array of $NaTaO_3$ nanoparticles via a confined space synthesis route and its photocatalytic application. Phys Chem Chem Phys 2011;13:2563–70. DOI: 10.1039/c0cp02141e

[47] Wu X, Yin S, Liu B, Kobayashi M, Kakihana M, Sato T. A carbon modified $NaTaO_3$ mesocrystal nanoparticle with excellent efficiency of visible light induced photocatalysis. J Mater Chem A 2014;2:20832–40. DOI: 10.1039/c4ta04132a

[48] Iwase A, Kato H, Kudo A. The effect of Au cocatalyst loaded on La-doped $NaTaO_3$ on photocatalytic water splitting and O_2 photoreduction. Appl Catal B: Environ 2013;136–137:89–93. DOI: 10.1016/j.apcatb.2013.02.006

[49] Jana P, Montero CM, Pizarro P, Coronado JM, Serrano DP, O'Shea VADLP. Photocatalytic hydrogen production in the water/methanol system using Pt/RE:$NaTaO_3$ (RE = Y, La, Ce, Yb) catalysts. Int J Hydrogen Energy 2014;39:5283–90. DOI: 10.1016/j.ijhydene.2013.12.182

[50] Husin H, Su WN, Pan CJ, Liu JY, Rick J, Yang SC, Chuang WT. Pd/NiO core/shell nanoparticles on $La_{0.02}Na_{0.98}TaO_3$ catalyst for hydrogen evolution from water and aqueous methanol solution. Int J Hydrogen Energy 2013;38:13529–40. DOI: http://dx.doi.org/10.1016/j.ijhydene.2013.07.116

[51] Gómez-solis C, Ruiz-Gómez MA, Torres-Martínez LM, Juárez-Ramírez I, Sánchez-Martínez D. Facile solvo-combustion synthesis of crystalline $NaTaO_3$ and its photocatalytic performance for hydrogen production. Fuel 2014;130:221–7. DOI: 10.1016/j.fuel.2014.04.019

[52] Ran J, Zhang J, Yu J, Jaroniec M, Qiao SZ. Earth-abundant cocatalysts for semiconductor-based photocatalytic water splitting. Chem Soc Rev 2014;43:7787–812. DOI: 10.1039/c3cs60425j

[53] Tsai CW, Chen HM, Liu RS, Asakura K, Chan TS. Ni@NiO core-shell structure-modified nitrogen-doped $InTaO_4$ for solar-driven highly efficient CO_2 reduction to methanol. J Phys Chem C 2011;115:10180–6. DOI: 10.1021/jp2020534

[54] Hu CC, Teng H. Structural features of p-type semiconducting NiO as a co-catalyst for photocatalytic water splitting. J Catal 2010;272:1–8. DOI: 10.1016/j.jcat.2010.03.020

[55] Husin H, Su WN, Chen HM, Pan CJ, Chang SH, Rick J, Chuang WT, Sheu HS, Hwang BJ. Photocatalytic hydrogen production on nickel-loaded $La_xNa_{1-x}TaO_3$ prepared by hydrogen peroxide-water based process. Green Chem 2011;13:1745–54. DOI: 10.1039/c1gc15070g

[56] Wen F, Li C. Hybrid artificial photosynthetic systems comprising semiconductors as light harvesters and biomimetic complexes as molecular cocatalysts. Account Chem Res 2013;46:2355–64. DOI: 10.1021/ar300224u

[57] Seo SW, Park S, Jeong HY, Kim SH, Sim U, Lee CW, Nam KT, Hong KS. Enhanced performance of $NaTaO_3$ using molecular co-catalyst $[Mo_3S_4]^{4+}$ for water splitting into H_2 and O_2. Chem Commun 2012;48:10452–4. DOI: 10.1039/c2cc36216c

[58] Kudo A, Kato H, Nakagawa S. Water splitting into H_2 and O_2 on new $Sr_2M_2O_7$ (M = Nb and Ta) photocatalysts with layered perovskite structures: factors affecting the photocatalytic activity. J Phys Chem B 2000;104:571–5. DOI: 10.1021/jp9919056

[59] Sugandha, Jha AK. Effect of the sintering temperature on nanocrystalline non-stoichiometric $Sr_{0.8}Bi_{2.2}Ta_2O_9$ ferroelectric ceramics. Ferroelectrics 2014;459:160–71. DOI: 10.1080/00150193.2013.849518

[60] Peng Z, Xing X, Chen X. Preparation and structure of a new layered organic-inorganic hybrid between the protonated form of a perovskite $Bi_2SrTa_2O_9$ and tetraphenylporphyrin by the intercalation behavior. J Alloys Compounds 2006;425:323–8. DOI: 10.1016/j.jallcom.2006.01.051

[61] Li Y, Chen G, Zhou C, Li Z. Photocatalytic water splitting over a protonated layered perovskite tantalate $H_{1.81}Sr_{0.81}Bi_{0.19}Ta_2O_7$. Catal Lett 2008;123:80–3. DOI: 10.1007/s10562-008-9397-5

[62] Nedelcu L, Toacsan MI, Banciu MG, Loachim A. Microwave properties of $Ba(Zn_{1/3}Ta_{2/3})O_3$ dielectric resonators. J Alloys Compounds 2011;509:477–81. DOI: 10.1016/j.jallcom.2010.09.069

[63] Park TK, Kim NK. Phase development in $Ba(Mg_{1/3}Ta_{2/3})O_3$ via conventional and B-site precursor routes. Ceramics Int 2008;34:1955–8. DOI: 10.1016/j.ceramint.2007.07.013

[64] Ling CD, Avdeev M, Kharton VV, Yaremchenko AA, Macquart RB, Hoelzel M. Structures, phase transitions, hydration, and ionic conductivity of $Ba_4Ta_2O_9$. Chem Mater 2010;22:532–540. DOI: 10.1021/cm903170t

[65] Xu TG, Zhang C, Shao X, Wu K, Zhu YF. Monomolecular-layer $Ba_5Ta_4O_{15}$ nanosheets: Synthesis and investigation of photocatalytic properties. Adv Funct Mater 2006;16:1599–607)DOI: 10.1002/adfm.200500849

[66] Shimizu K, Itoh S, Hatamachi T, Kitayama Y, Kodama. Pillaring of Ruddlesden–Popper perovskite tantalates, $H_2ATa_2O_7$ (A = Sr or $La_{2/3}$), with n-alkylamines and oxide nanoparticles. J Mater Chem 2006;16:773–9. DOI: 10.1039/B514066H

[67] Ikeue K, Mitsuyama T, Arayama K, Tsutsumi A, Machida M. Effect of heat treatment on local structure and photocatalytic water splitting activity of Ni-loaded Li-$Ca_2Ta_3O_{10}$. J Ceramic Soc Jpn 2009;117:1161–5. DOI: doi.org/10.2109/jcersj2.117.1161

[68] Yoshioka K, Petrykin V, Kakihana M, Kato H, Kudo A. The relationship between photocatalytic activity and crystal structure in strontium tantalates. J Catal2005;232:102–7. DOI: 10.1016/j.jcat.2005.02.021

[69] Ikeda S, Fubuki M, Takahara YK, Matsumura M. Photocatalytic activity of hydrothermally synthesized tantalate pyrochlores for overall water splitting. Appl Catal A: Gen 2006;300:186–90. DOI: 10.1016/j.apcata.2005.11.007

[70] Babooram K, Ye ZG. New soft chemical routes to ferroelectric $SrBi_2Ta_2O_9$. Chem Mater 2006;18:532–40. DOI: 10.1021/cm051866c

[71] Wang W, Ke H, Rao JC, Feng M, Zhou Y. Sol-Gel synthesis of $SrBi_2Ta_2O_9$ nanowires. J Alloys Compound 2010;504:367–70. DOI: 10.1016/j.jallcom.2010.05.118

[72] Inaba K, Suzuki S, Noguchi Y, Miyayama M, Toda K, Sato M. Metastable $Sr_{0.5}TaO_3$ perovskite oxides prepared by nanosheet processing. Euro J Inorg Chem 2008;2008(35):5471–5. DOI: 10.1002/ejic.200800776

[73] Li M, Zhang J, Dang W, Cushing SK, Guo D, Wu N, Yin P. Photocatalytic hydrogen generation enhanced by band gap narrowing and improved charge carrier mobility in $AgTaO_3$ by compensated co-doping. Phys Chem Chem Phys 2013;15:16220–6. DOI: 10.1039/C3CP51902C

[74] Nyman M, Rodriguez MA, Rohwer LES, Martin JE, Waller M, Osterloh FE. Unique $LaTaO_4$ polymorph for multiple energy applications. Chem Mater 2009;21:4731–7. DOI: 10.1021/cm9020645

[75] Shimizu K, Itoh S, Hatamachi T, Kodama T, Sato M, Toda K. Photocatalytic water splitting on Ni-intercalated Ruddlesden-Popper tantalate $H_2La_{2/3}Ta_2O_7$. Chem Mater 2005;17:5161–6. DOI: 10.1021/cm050982c

[76] Tsujimoto Y, Yamaura K, Muromachi ET. Oxyfluoride chemistry of layered perovskite compounds. Appl Sci 2012;2:206–19. DOI: 10.3390/app2010206

[77] Bao NZ, and Arunava G. Inorganic spintronic materials. Encyclo Inorg Bioinorg Chem 2004;03:01–15.

[78] Miseki Y, Kato H, Kudo A. Water splitting into H_2 and O_2 over niobate and titanate photocatalysts with (111) plane-type layered perovskite structure. Energy Environ Sci 2009;2:306–14. DOI: 10.1039/B818922F

[79] Bharti C, Sinha TP. Synthesis, structure and dielectric properties of a rare earth double perovskite oxide Ba_2CeTaO_6. Mater Res Bull 2011;46:1431–6. DOI: 10.1016/j.materresbull.2011.05.007

[80] Ibberson RM, Moussa SM, Rosseinsky MJ, Fitch AN, Iddles D, Price T. In situ neutron and X-ray powder diffraction study of cation ordering and domain growth in the dielectric ceramic $Ba_3ZnTa_2O_9$-Sr_2GaTaO_6. J Am Ceramic Soc 2006;89:1827–33. DOI: 10.1111/j.1551-2916.2006.01047.x

[81] Rajendran DN, Nair KR, Rao PP, Sibi KS, Koshy P, Vaidyan VK. New perovskite type oxides: $NaATiMO_6$ (A=Ca or Sr; M=Nb or Ta) and their electrical properties. Mater Lett 2008;62:623–8. DOI: 10.1016/j.matlet.2007.06.022

[82] Chen S, Yang J, Ding C, Li R, Jin S, Wang D, Han H, Zhang F, Li C. Nitrogen-doped layered oxide $Sr_5Ta_4O_{15-x}N_x$ for water reduction and oxidation under visible light irradiation. J Mater Chem A 2013;1:5651–9. DOI: 10.1039/C3TA10446J

[83] Mukherji A, Sun C, Smith SC, Lu GQ, Wang L. Photocatalytic hydrogen production from water using N-doped $Ba_5Ta_4O_{15}$ under solar irradiation. J Phys Chem 2011;115:15674–8. DOI: 10.1021/jp202783t

[84] Guo Z, Sa B, Pathak B, Zhou J, Ahuja R, Sun Z. Band gap engineering in huge-gap semiconductor $SrZrO_3$ for visible-light photocatalysis. Int J Hydrogen Energy 2014;39:2042–8. DOI: 10.1016/j.ijhydene.2013.11.055

[85] Liu P, Nisar J, Ahuja R, Pathak B. Layered perovskite $Sr_2Ta_2O_7$ for visible light photocatalysis: a first principles study. J Phys Chem C 2013;117:5043–50. DOI: 10.1021/jp310945e

[86] Marschall R, Soldat J, Wark M. Enhanced photocatalytic hydrogen generation from barium tantalate composites. Photochem Photobiol Sci 2013;12:671–7. DOI: 10.1039/C2PP25200G

[87] Mukherji A, Seger B, Lu GQ, Wang L. Nitrogen doped $Sr_2Ta_2O_7$ coupled with graphene sheets as photocatalysts for increased photocatalytic hydrogen production. ACS Nano 2011;5:3483–92. DOI: 10.1021/nn102469e

[88] Iwase A, Kato H, Kudo A. Nanosized Au particles as an efficient cocatalyst for photocatalytic overall water splitting. Catal Lett 2006;108:7–10. DOI: 10.1007/s10562-006-0030-1

[89] Hagiwara H, Inoue T, Kaneko K, Ishihara T. Charge-transfer mechanism in Pt/$KTa(Zr)O_3$ photocatalysts modified with porphyrinoids for water splitting. Chem – Euro J 2009;15:12862–70. DOI: 10.1002/chem.200901772

[90] Sreethawong T, Ngamsinlapasathian S, Suzuki Y, Yoshikawa S. Nanocrystalline mesoporous Ta_2O_5-based photocatalysts prepared by surfactant-assisted templating sol-gel process for photocatalytic H_2 evolution. J Molecul Catal A – Chem 2005;235:1–11. DOI: 10.1016/j.molcata.2005.03.021

[91] Chen X, Chen W, Gao H, Yang Y, Shangguan W. In situ photodeposition of NiO_x on CdS for hydrogen production under visible light: Enhanced activity by controlling solution environment. Appl Catal B: Environ 2014;152–153:68–72. DOI: 10.1016/j.apcatb.2014.01.022

[92] Jorge AB, Martin DJ, Dhanoa MTS, Rahman AS, Makwana N, Tang J, Sella A, Corà F, Firth S, Darr JA, McMillan PF. H_2 and O_2 evolution from water half-splitting reactions by graphitic carbon nitride materials. J Phys Chem C 2013;117:7178–85. DOI: 10.1021/jp4009338

[93] Wang J, Li B, Chen J, Li N, Zheng J, Zhao J, Zhu Z. Enhanced photocatalytic H_2-production activity of $Cd_xZn_{1-x}S$ nanocrystals by surface loading MS (M = Ni, Co, Cu) species. Appl Surface Sci 2012;259:118–23. DOI: 10.1016/j.apsusc.2012.07.003